The interaction between a sonic jet and an oblique shock wave in a supersonic crossflow

Dacome, G.; Schrijer, F.F.J.; van Oudheusden, B.W.

The interaction between a sonic jet and an oblique shock wave in a supersonic crossflow

Giulio Dacome*, Ferry F.J. Schrijer† and Bas W. van Oudheusden‡
Delft University of Technology, 2629HS Delft, The Netherlands

The current study considers the configuration of a transverse jet in a supersonic crossflow that is interacting with an impinging oblique shock wave. The relevance of this configuration is associated to high-speed air-breathing propulsion systems, where a shock may be induced in the combustion chamber to enhance mixing. To investigate the behaviour of this system, experiments were conducted in a supersonic test facility at a freestream Mach number of 2, analyzing the effect of three main control variables: the jet momentum flux ratio, the shock strength and the impingement position of the shock on the jet plume. Measurements were acquired using surface oil-flow visualization, schlieren photography and Particle Image Velocimetry. Results reveal that near-field momentum-driven mixing remains largely unaffected after the introduction of the impinging shock wave, while mid-to-far-field mixing mechanisms do change. An increase in jet plume elevation was observed, as well as the formation of a strong shear layer downstream of the jet, which acts as a source of vorticity that promotes entrainment towards the jet mid-field. A stronger shock wave was found to be more beneficial for mixing performance. This effect was seen to decrease with weakening shock strength or by shifting the strong shock further downstream.

I. Nomenclature

d	=	jet diameter [m]
J	=	momentum flux ratio [-]
M	=	Mach number [-]
p	=	static pressure [Pa]
u	=	x-component of velocity [m/s]
V	=	magnitude of velocity [m/s]
x	=	streamwise coordinate [m]
y	=	wall-normal coordinate [m]
z	=	spanwise coordinate [m]
γ	=	specific heat ratio [-]
ε	=	uncertainty
θ	=	flow deflection angle [deg]
ρ	=	fluid density [kg/m^3]
ω	=	vorticity [1/s]

Acronyms

CVP	=	Counter-rotating Vortex Pair
OSW	=	Oblique Shock Wave
PIV	=	Particle Image velocimetry
SBLI	=	Shock Wave Boundary Layer Interaction
TKE	=	Turbulent Kinetic Energy

---
*Ph.D. Candidate, Faculty of Aerospace Engineering
†Assistant Professor, Faculty of Aerospace Engineering
‡Associate Professor, Faculty of Aerospace Engineering

II. Introduction

As air-breathing propulsion is promising to make its appearance in high-speed transport and orbital insertion, Supersonic Combustion ramjet (SCramjet) engines offer the highest efficiency for flight in the hypersonic regime [1]. One of the most effective combustion chamber designs that has been considered in legacy work and recent literature is the relatively simple concept of a transverse jet injected into a (supersonic) crossflow. With virtually no moving parts and the enthalpy of the incoming supersonic stream allowing for auto-ignition and spontaneous combustion, this engine configuration promises to deliver the best system performance. Momentum-driven effects being prominent in the near-field and diffusion-based ones in the far-field, this injection system holds many advantages.

The anatomy of a jet in a crossflow has been extensively studied in previous literature, such as in Ref. [2] for subsonic conditions and by Refs. [3] and [4] for supersonic flow conditions. Special attention in the literature has been devoted to the determination of scaling laws for the jet trajectory, such as in Refs. [5], [6] and [7]. In the context of combustor design, plume elevation above the wall determines the heat flux to the wall, thus dictating requirements for the structural design of the chamber [8]. For mixing in a combustion chamber, though, plume elevation is not the sole performance indicator.

To obtain combustion fuel and air need also to be mixed in the proper mass ratio. A way to enhance entrainment and, consequently, mixing of the two perpendicular fluid streams is the introduction of an oblique shock wave impinging on the jet plume [9, 10]. This enhances mixing by introducing a source of baroclinic vorticity as well as increasing static temperature and pressure. Previous work in the field reported on the near-wall flow patterns of combustors with other mixing enhancement techniques [11], and on ways to make use of a transverse jet on the control of a shock-wave boundary-layer interaction (SBLI) [12]. The addition of an oblique shock wave (OSW) is expected to greatly enhance the mixing performance by generating vorticity and promoting the formation of small-scale turbulent structures and increasing the turbulence mixing intensity. The general characteristics of the additional interaction caused when an oblique oblique shock wave impinges on a surface boundary layer have been relatively well documented, such as in Refs. [13] or [14], under conditions where it occurs in relative isolation. In contrast, the interaction with an upstream jet blowing air away from the wall causes relatively unknown effects to the interaction domain of the SBLI. As mentioned by Ref. [15], blowing air perpendicular to the boundary layer renders it unstable, potentially anticipating separation, which could be worsened by the introduction of a shock wave impinging downstream. Yet, further studies, such as Ref. [16], analysing the interaction between a recirculation channel (thus resulting in a jet upstream of the shock) show how such configuration can prove beneficial for shortening the length of the separation region caused by the SBLI. However, in that case, the jet was driven by the pressure difference between the conditions downstream of the shock and the ones upstream of it. More experimental studies have been documented in literature that investigate the interaction between a jet in crossflow driven by an external pressure source and an incident shock wave or between streamwise vortices (such as the jet-induced Counter-rotating Vortex Pair, or CVP) and an oblique shock [17, 18]. Even though some studies [9, 19] prove that positioning the impingement location of the shock downstream of the injector is beneficial for reducing the separation length in the SBLI region, there is little evidence of how the mixing properties are affected by the shock position.

The goal of this research project is to investigate the fluid-dynamic performance of such a combustor design. Experiments were carried out in a simplified (cold flow) representation to provide a theoretical baseline for the behaviour of the flow in such a configuration, in an attempt to quantify the effect of several design variables on the mixing performance. This is accomplished by analysing the interaction in terms of flow topology, reconstructed velocity fields from Particle Image Velocimetry measurements, as well as vorticity and Reynolds stress fields. Parametrically, this translates to the study of different combinations of incident shock strength, impingement position and jet momentum flux ratio. This last variable is one of the most relevant governing parameters of any jet-in-crossflow system and is defined as the ratio of dynamic pressures of jet-to-crossflow conditions (Eq. 1).

$$J = \frac{\rho_{\text{jet}} u_{\text{jet}}^2}{\rho_\infty u_\infty^2} = \frac{\gamma_{\text{jet}} p_{\text{jet}} M_{\text{jet}}^2}{\gamma_\infty p_\infty M_\infty^2} \tag{1}$$

The momentum flux ratio has a primary effect on the trajectory of the jet itself and on its penetration, while the incoming boundary layer has an additional but less prominent influence [4]. Both these aspects depend furthermore on the Mach number of the cross stream.

III. Experimental Methodology

A. Supersonic Facility and Set-up

The experiments were carried out in the ST-15 supersonic tunnel of TU Delft, which is a blowdown facility with a test section size of 15×15 cm^2, at a freestream Mach number of $M_\infty = 2$ and a stagnation pressure of $p_0 = 2$ bar. The flow is accelerated isentropically to the test Mach number. The transverse jet system was installed below a flush-mounted plate in the bottom wall of the test section as shown in Figure 1. Either strong or a weak oblique shock (with flow deflection angles of $\theta = 12$ deg and $\theta = 9$ deg, respectively) were introduced in the flow, for two different impingement positions: $x_{\text{shock}}/d_{\text{jet}} = 13$ and $x_{\text{shock}}/d_{\text{jet}} = 16$, where x_{shock} is the extrapolated intersection of the impinging shock and the test section wall in inviscid conditions, measured downstream from the jet. For this purpose, wedge-shaped shock generators were installed on the upper wall for the two deflection angles considered. These could slide upstream or downstream depending on the desired position of the shock impingement line. The boundary layer thickness in the empty test section (without the jet and the impinging shock) is 5 mm and is fully turbulent.

Fig. 1 Test section of the ST-15 supersonic facility. Mach-2 nozzle installed and plate with transverse jet positioned for testing indicated with red circle.

A transverse jet was injected at sonic outlet conditions ($M_{\text{jet}} = 1$) and varying momentum flux ratio ($J = 1$ and $J = 2$). The jet air supply was provided with an assembly including a pressure regulator to set the momentum flux ratio. Pressurised air was supplied through a series of feeding lines and a 90-degree bend pipe and issued perpendicular into the supersonic stream in the test section. The jet injector system also featured an insert for an additional line to feed seeding for PIV imaging. The jet nozzle exit diameter $d_{\text{jet}} = 4$ mm and has been used as the reference length to nondimensionalize parameters, even in the case when no jet is operated. Figure 2 shows a schematic of the test setup, with most relevant dimensions indicated. Table 1 reports the range of parameters in use during the testing.
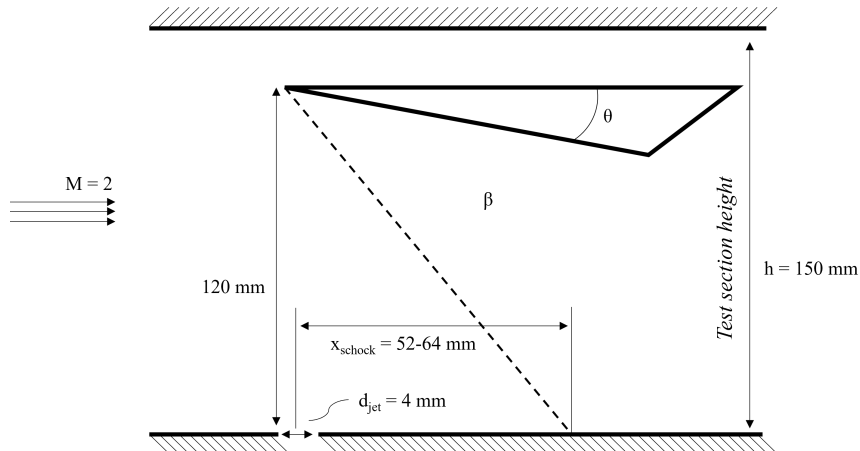
Fig. 2 Schematic of the test set-up in the supersonic facility

3

M_∞	$p_{0,\infty}$	T_0	$p_{0,\mathrm{jet}}$	$T_{0,\mathrm{jet}}$	M_{jet}	Re_{jet}	θ	$x_{\mathrm{shock}}/d_{\mathrm{jet}}$
2	2 [bar]	295 [K]	2 [bar] (J=1)	298 [K]	1	59,000	9 [deg]	13
			4 [bar] (J=2)				12 [deg]	16

Table 1 Testing parameters in use for the freestream and the jet conditions as well as the geometry of the incident shock waves

B. Qualitative flow visualization techniques

Schlieren and shadowgraphy as well as oil flow visualization were conducted to quantify the basic geometric properties of the flow field emerging from the interaction. These measurements provided an initial exploration, on the basis of which conditions were selected for a more detailed investigation with stereo particle image velocimetry (PIV).

The oil flow visualization was performed with a mixture of titanium dioxide particles and an organic oil. This allowed to visualize the near-wall flow structures and the qualitative effects of the shock wave on the jet-crossflow interaction.

The set-up for schlieren and shadowgraphy saw the optics arranged in a Z-type configuration. Here, a lens with a focal length of 100 mm collimated the light emanating from the LED source into a convex lens followed by the pin hole. On the other side of the test section, a Photron FastCAM SA1.1 camera with a resolution of 1024×1024 pixels was used for image capture with an acquisition frequency of 60 Hz and a shutter speed of 1/12,000 s for most measurements. The focal length of the camera lens was set at 500 mm.

C. Stereo PIV

The majority of the experimental effort was dedicated to stereoscopic particle image velocimetry (Stereo PIV) measurements. This was accomplished both on wall-normal and wall-parallel planes. The reason behind the use of dual imaging plane orientations was the intention to not only study the interaction in the expected symmetry plane of the interaction, but also capture potential spanwise-oriented phenomena resulting from the inherent three-dimensionality of the flow problem at hand. The impingement of the oblique shock wave is, in fact, expected to deeply alter some of the structures which are typical of a canonical jet in crossflow interaction, such as the CVP.

DEHS particles were used to seed both the freestream flow and the transverse jet flow. Seeding is generated by two PIVTech PIVPart 45 seeders, each operating with an overpressure of 1 bar with respect to the corresponding ambient pressure (jet or freestream). The seeding is approximately 1 μm in size and is introduced in the settling chamber to seed the wind tunnel freestream and directly fed into the jet supply assembly as well.

Two LaVision sCMOS cameras with a resolution of 2560×2160 pixels were used to capture the particle images acquiring image pairs with a time separation of 0.6 μs at a sampling frequency of 15 Hz. Wall-normal planes were imaged with a focal length of 105 mm and a magnification factor of 0.28, whereas wall-parallel views saw values of 60 mm and 0.27 for the aforementioned parameters, respectively. The f-stop was set at 11 for both cases. A field of view with a streamwise extent of 100 mm was imaged in either case.

Illumination was provided by a Quantel Evergreen Nd:YAG laser oprated in double-pulse mode at a repetition frequency of 15 Hz, with a pulse energy of 200 mJ, and a luminous wave length of $\lambda = 532$ nm. The laser beam was introduced into the test section from the diffuser downstream of the test section with the aid of a mirror placed in a probe. Figure 3 displays the optical configuration for both the wall-normal and wall-parallel cases. Four imaging planes were studied: two wall-normal planes at $z/d_{\mathrm{jet}} = 0$ and $z/d_{\mathrm{jet}} = 2$ and two wall-parallel ones at $y/d_{\mathrm{jet}} = 1$ and $y/d_{\mathrm{jet}} = 2$.

The particle images were processed with the aid of Davis 8.4. Processing was performed with a multi-pass method: the first pass was conducted with a window size of 64×64 pixels and a circular window shape. Two more passes were carried out with a square interrogation window of size 32×32 pixels. Interrogation window overlap was set at 75%, resulting in a final vector pitch of one vector every 0.93 mm. The obtained vector data was processed to yield fields of mean velocity, standard deviation and further second-order statistics (such as Reynolds stresses). Due to the proximity to the wall and the inherent vector resolution resulting from the cross-correlation processing, a layer of about one window height cannot be analysed in the proximity of the bottom liner. Particle densities were measured to be between 0.073 particles per pixel (ppp) and 0.081 ppp for both the wall-normal and wall-parallel imaging configurations, although some variation between the wake and freestream regions was observed, especially for the wall-normal acquisitions (see Figure 4).
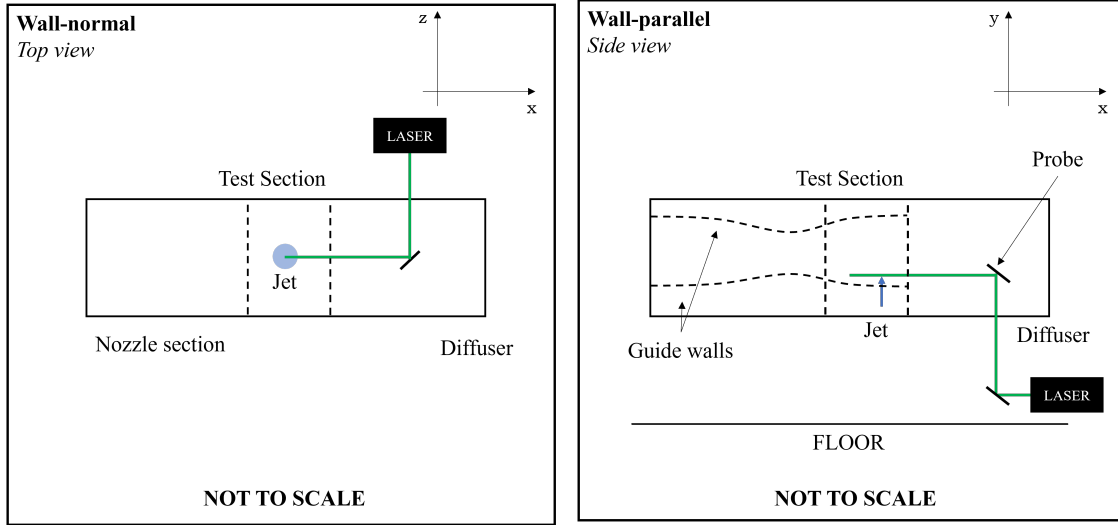
Fig. 3   Schematic displaying how the laser is introduced in the test section.
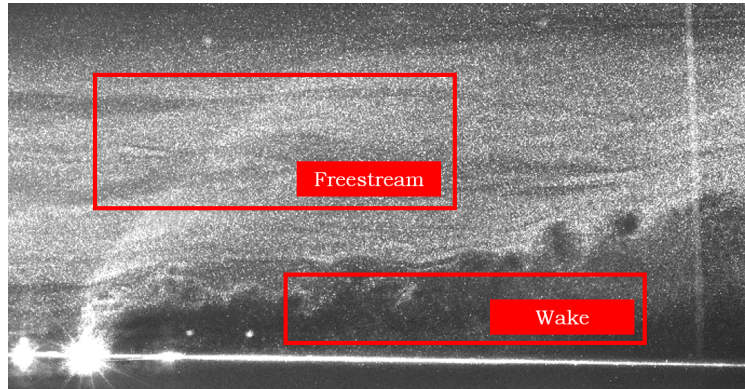

Fig. 4   Particle image acquired with $J = 1$ and no impinging shock wave displaying the two regions of interest with different particle density.

D. PIV measurement uncertainty

Stereo PIV is affected by uncertainty in the measurement of the out-of-plane velocity component, in relation to the viewing angles of the cameras, which was 48 deg and 84 deg for the wall-parallel and wall-normal acquisitions, respectively. This results in a error ratio of out-of-plane to in-plane components of roughly unity for wall-parallel acquisitions and of the order of 2-3 for the wall-normal ones. Additionally, sources of uncertainty in the reconstruction of the velocity field can derive from particle slip, window size, the cross-correlation operator and the sample size of the image set. Table 2 provides an overview of the several errors arising from each of these factors.

IV. Results

The complexity of the interaction between the transverse jet, the impinging shock wave and the Mach-2 external flow calls for a comparison of such phenomenon with the baseline flow cases which the whole field is a combination of. These are essentially the jet in supersonic crossflow (without impinging shock) and the flow field generated by an oblique shock interacting with the boundary layer (without jet interaction). Once the juxtaposition is clear, it is possible to investigate how some of the aspects of the jet in crossflow are affected by the introduction of the impinging shock, for instance its trajectory and the Reynolds stresses induced in the field.

Error source	Symbol	Wall-normal	Wall-parallel
u-component	ε_u	<0.088 [m/s]	<0.521 [m/s]
v-component	ε_v	<0.121 [m/s]	<0.623 [m/s]*
w-component	ε_w	<0.198 [m/s]*	<0.523 [m/s]
RMS - u	$\varepsilon_{u'}$	<0.067 [m/s]	<0.260 [m/s]
Vorticity	ε_ω	<23.8 [1/s]	<31.6 [1/s]
Particle slip	ε_{slip}	<3.01 [m/s]	<7.54 [m/s]
Window size	ε_{ws}	<-3.64E-4 [m/s]	<3.64E-4 [m/s]
Cross-correlation	ε_{cc}	<7.73 [m/s]	<8.02 [m/s]

Table 2   PIV uncertainty. Values marked by (*) refer to the out-of-plane velocity.

A. Baseline configurations: jet in crossflow and SWBLI

As the transverse jet enters the supersonic crossflow in the test section, it is enveloped in a barrel shock that terminates with a Mach disk [3, 4]. This last feature is of utmost importance for the momentum-driven mixing in the near-field and its location above the wall is a good measure of the mixing performance in this region of the flow field [20]. Its position was found to move away from the wall and shift downstream almost linearly with increasing jet momentum flux ratio, as expected from literature [21]. Figure 5 shows the schlieren visualization of the interaction in one of the baseline configurations (i.e. with no oblique shock impingement).
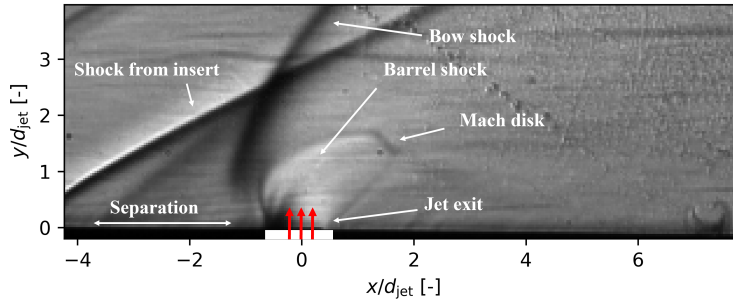

Fig. 5   Schlieren image of the sonic jet in crossflow with $J = 1$ and $M_\infty = 2$.

The schlieren image also highlights some other aspects of the interaction between the jet and the crossflow. Upstream of the injection port, compression waves form which coalesce into the upstream bow shock. This results from the separation induced by the transverse momentum injected by the jet into the crossflow [22]. A secondary compression wave is visible in the image upstream which originates from the seam of the plate insert, but which is irrelevant for the flow of interest. To better investigate the behaviour of the flow downstream of the injector, Figure 6 illustrates the corresponding velocity field as obtained from PIV measurements.

The transverse momentum injection into the flow by the jet causes a considerable loss of momentum of the flow downstream of the injector. Towards the end of the field of view a large portion of the flow is furthermore characterized by rather low velocity due to the growth of the boundary layer. Also, an expansion fan forms above the jet Mach disk that accelerates the flow again after injection.

The evolution of the flow field in a wall-parallel plane allows to visualize the development of the CVP. In such a representation, the CVP appears as two streaks of reduced velocity due to the momentum loss caused by the jet. A visualization of the spanwise velocity component will, instead, show two regions of velocity of opposite sign (as in Figure 7). The introduction of the incident oblique shock wave is expected to distort the spatial (especially streamwise) evolution of the CVP. More on this will be discussed in the next section of the paper.

Figure 7 also highlights some other aspects of the field. For instance, a secondary shock forms downstream of the main bow shock because of the circulation of fluid around the jet and consequent reattachment right downstream of the orifice. This results in an inversion of the sign of the spanwise velocity upon crossing of this secondary shock.
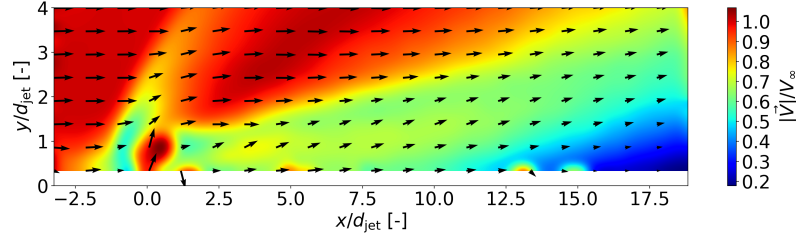
Fig. 6 **Ensemble-averaged PIV image captured for $M_\infty = 2$, $M_{\mathrm{jet}} = 1$ and $J = 1$. Coloured by velocity magnitude.**
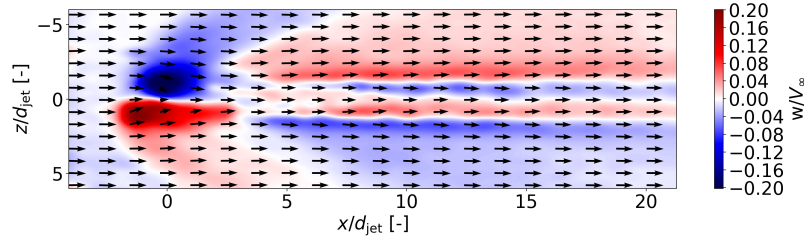
Fig. 7 **Velocity field on wall-parallel plane located at $y/d_{\mathrm{jet}} = 1$ with $J = 1$ and $M_\infty = 2$. Coloured by spanwise velocity component (w).**
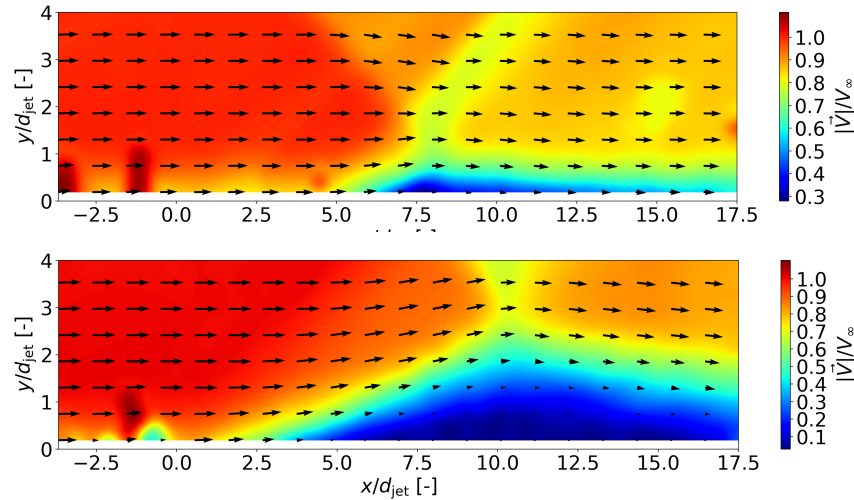

Fig. 8 **Velocity field of impinging oblique shock generated from 9-deg flow deflection (top) and 12-deg flow deflection. Coloured by velocity magnitude.**

As the complementary baseline case, Figure 8 shows the velocity fields generated by the interaction of a shock with the boundary layer, in absence of jet injection. Both the fields resulting from a flow deflection of either $\theta = 9\,\mathrm{deg}$ or $\theta = 12\,\mathrm{deg}$ are shown. The reference (inviscid) shock impingement position is $x/d = 10$ for the weak case and $x/d = 13$ for the strong one. A region of considerably low velocity then naturally emerges in the boundary layer in the proximity of the point of impingement of the shock, creating an upstream compression wave whose onset is located $5d_{\mathrm{jet}}$ upstream of the inviscid shock foot. The interaction does not appear to lead to large-scale separation or flow blockage. The interaction with a stronger shock with $\theta = 12\,\mathrm{deg}$ (Figure 8), instead, appears to cause a much more noticeable interaction region, with the onset of the compression wave now $8.5d_{\mathrm{jet}}$ upstream of the shock foot. This has a drastic effect on the boundary layer recovery and the trajectory of the jet in crossflow, as will be analysed in a later section.

7

B. Flow topology with impinging oblique shock wave on the jet in crossflow

Figure 9 displays the interaction field of the jet in crossflow and the impinging oblique shock wave. On the upstream (left-hand) side, the barrel shock appears clearly visible together with the distinctive Mach disk as well as the bow shock formed upstream. Downstream of the jet, instead, a λ-type shock-wave boundary-layer interaction zone appears close to the impingement of the incoming shock (at $x_{\text{shock}}/d_{\text{jet}} \approx 6$). With the shock impinging downstream of the injector and considering that most of the flow is supersonic downstream of the barrel shock, no considerable effect of the shock on the near-field jet interaction properties is observed, apart from the alteration of the length of the separation zone downstream of the jet. The length of this region increases as the shock is inserted into the flow field (more details will be presented in one of the next sections).
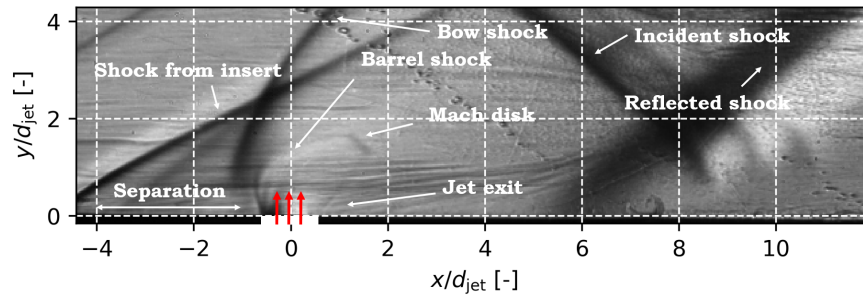
Fig. 9 Ensemble-averaged schlieren photograph captured at $M_\infty = 2$, $M_{\text{jet}} = 1$, $J = 2$, $\theta = 9\deg$ **and** $x_{\text{shock}}/d_{\text{jet}} = 13$.

An oil flow visualization of the flow with emphasis on the near-field of the jet is displayed in Figure 10 for the same conditions as for the schlieren image in Figure 9, compared to the corresponding baseline configuration without impinging shock. The oil flow pattern displays the typical footprint of an "undisturbed" jet in crossflow up to $\approx 2 - 3d_{\text{jet}}$ downstream of the injection location. Three-dimensional SBLI interaction features caused by the interaction of the upstream bow shock with the boundary layer are visible in close proximity of the jet where flow recirculation is present [23], as well as the mild evolution of a collision shock downstream of the jet [24]. Also, large-scale wall-normal vortices appear close to the centre line of the interaction zone of the jet with the crossflow, upstream of the shock impingement position. These are believed to form due to the shear between the inner and outer regions of this zone. These structures also appear in the wall-parallel PIV measurements up to $y/d_{\text{jet}} = 1$. The strength of these vortices appears to drastically reduce with wall-normal distance as PIV fails to capture their presence at the higher position of $y/d_{\text{jet}} = 2$.
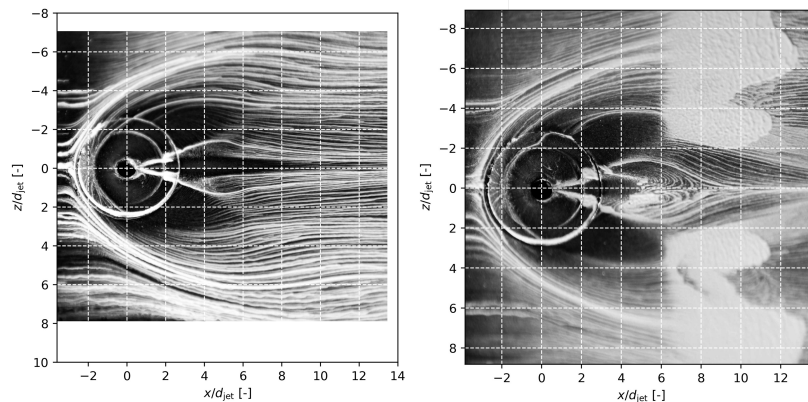
**Fig. 10 Wall oil flow visualization for** $M_\infty = 2$, $M_{\text{jet}} = 1$, $J = 2$ **with no impinging shock (left) and** $M_\infty = 2$, $M_{\text{jet}} = 1$, $J = 2$, $\theta = 9\deg$ **and** $x_{\text{shock}}/d_{\text{jet}} = 13$ **(right).**

C. Jet trajectory

The penetration of the jet into the crossflow is an important measure of the mixing potential and entrainment of the injected fluid into the surrounding stream. The higher the trajectory of the jet, the more opportunity the two fluids have to mix. The jet trajectory is determined by tracking the centreline of the jet across the flow field, which is approximated by a streamline generated from interpolation between nearby velocity vectors, using a first order integration scheme.

Analysis of the effect of the shock on the jet trajectory allows to investigate the change in how the plume penetrates into the crossflow and, correspondingly, allows for a better mixing. A comparison of the jet trajectories for the different shock/jet configurations is displayed in Figure 11. The baseline cases where the jet underwent no interference from the incident oblique shock are shown as solid lines. They show a rapid increase in penetration height directly following injection due to the transverse momentum transfer. This rising trend first levels off, after which it resumes its increase at about $x/d = 6$, where the effect of the CVP becomes dominant. The weak shock cases ($\theta = 9$ deg) show marginal to nill improvement with respect to the baseline. The curve for $J = 1$ even appears to have a lower penetration compared to its baseline counterpart. The higher-J case, instead, features a marginally higher elevation up until the location where the plume meets the incoming shock (marked with a small circle in Figure 11). From there on, the flow is again mostly parallel to the wall, as the development of the CVP is interrupted by the oblique shock. For the strong cases, the increase in elevation is much more pronounced. The combined effect of the CVP and the compression wave induced by the separation region cause the plume to rise abruptly in the near field. It can be speculated that the dominating effect here is not the CVP's action, but rather the upstream compression resulting from the SBLI at the oblique shock impingement location. Indeed, as the large-scale interaction region joins the incoming shock, the wall-normal velocity component becomes negative, deflecting the plume back down towards the wall.
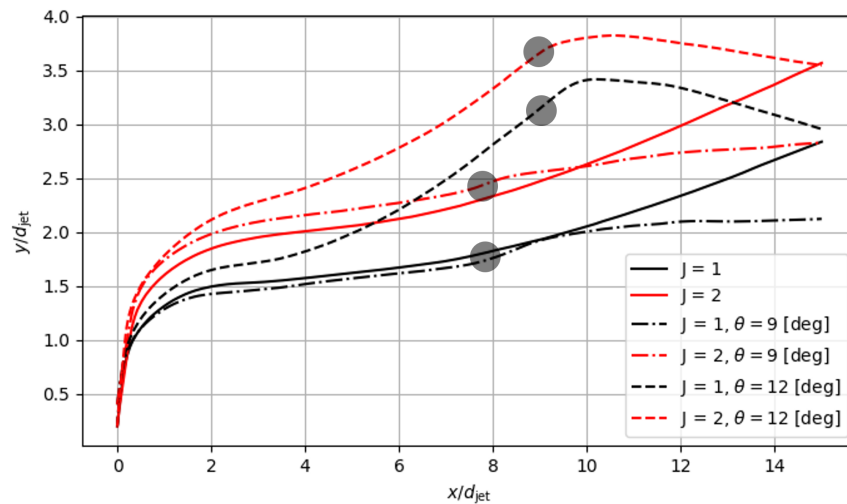

Fig. 11   Comparison of plume's centre line trajectory: showing cases with no shock as well as for $\theta = 9$ [deg] and $\theta = 12$ [deg] shocks impinging at $x/d = 12$. Approximate crossing of impinging shock marked with a grey circle.

D. The effect of shock impingement on mixing

Figure 12 reports the out-of-plane vorticity component in the wall-normal plane ($z = 0$), for the cases where the OSW (generated by either a 9-degree or 12-degree deflection) impinges on the bottom wall at $x/d = 13$, for a jet momentum flux ratio of $J = 1$. The development of a strong shear layer alongside the trajectory (between $x/d \approx 2.5$ and $x/d \approx 7.5$) in the near-field appears evident for both shock strengths. The 12-degree case, however, displays larger magnitude of vorticity in the shear layert. In fact, the weak case shows a similar vorticity field compared to baseline no-shock case; only to be interrupted by the formation of the SBLI interaction region in the mid-field. The strong case, instead, shows a different development pattern already in the immediate downstream vicinity of the jet. This suggests a possible increase in magnitude of the interaction mechanism and it is reasonable to conclude that this case corresponds to a stronger interaction region compared to the baseline. Figure 13 shows horizontal profiles of spanwise vorticity, extracted at

9

different elevations. The comparison clearly highlights how the bow shock creates a peak in vorticity, especially at low elevations, it being a source of baroclinic vorticity. Furthermore, at a height of 2 and 3 jet diameters, the curve for the 12-degree flow deflection shows a drastic drop in the region where the λ-shock structure forms due to the interaction with the boundary layer. Although this flow feature may suggest to promote entrainment towards the mid-field, it still does not provide definitive evidence of the true mixing performance. To investigate this phenomenon further, a more detailed discussion of the jet trajectory, as well as the spatial distribution Reynolds stresses is therefore undertaken.
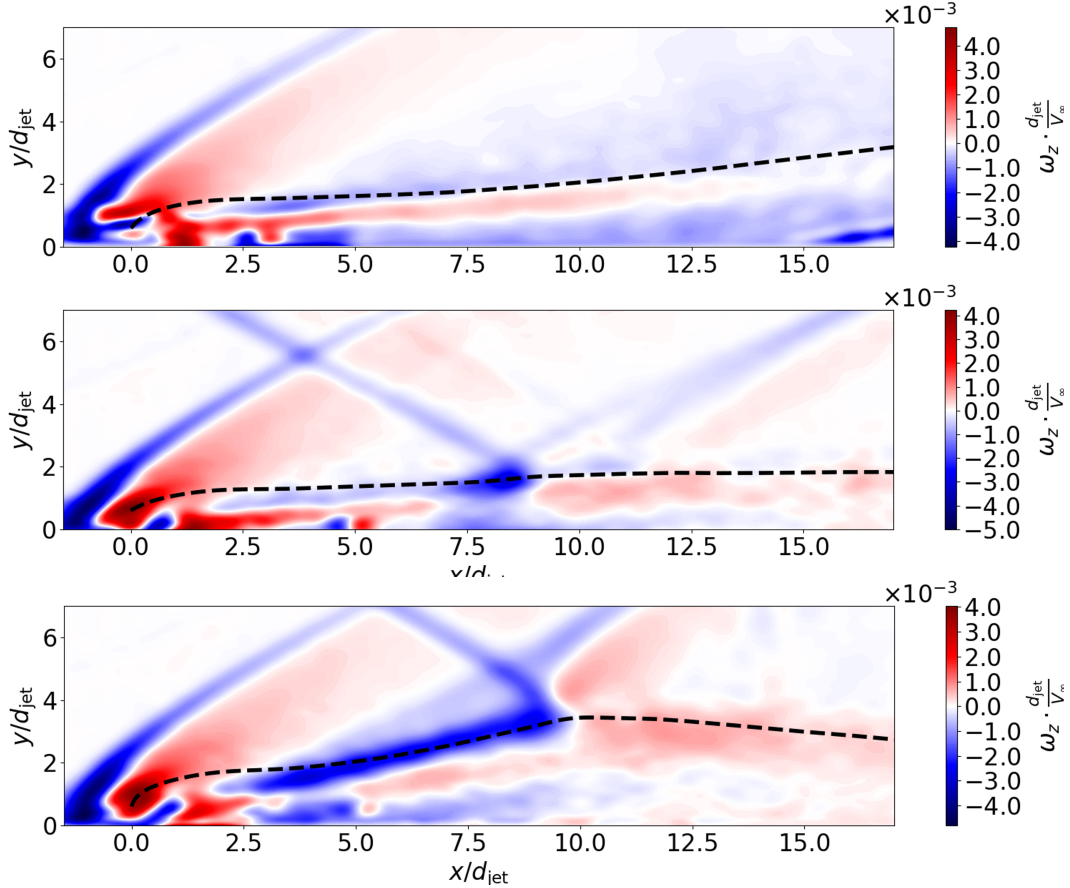

Fig. 12   Contour plots reporting the vorticity field for $J = 1$ **without shock impingement (top),** $J = 1$, $\theta = 9 \deg$ **(middle),** $\theta = 12 \deg$ **(bottom) and shock impingement position of** $x/d = 13$. **Jet rajectory marked with dashed line.**

Literature shows [25] how the development of a vortex is abruptly interrupted by the encounter with a shock. Analysis of the present results suggests that the CVP looses almost completely its strength upon crossing the impinging shock front. This effect is rather evident when the interaction occurs with the 9-degree flow deflection, where the plume stabilizes downstream of $x/d_{\text{jet}} \approx 10$, as Figure 12 (middle) displays. As the plume crosses, the 12-degree shock, instead, the trajectory appears to drop, indicating an almost complete loss in CVP strength, at least in the mid-field. Because of the limited extent of the field of view in the present investigation, no information is available on the further evolution of the trajectory in the far field.

Finally, the investigation of the spatial distribution of turbulent kinetic energy (presented in Figure 14) allows to identify the regions in the field which are characterized by most intense mixing. The turbulent kinetic energy is defined as Eq. 2.

$$TKE = \frac{1}{2} \left(\overline{u'u'} + \overline{v'v'} + \overline{w'w'} \right)$$ (2)

The spatial distribution of turbulent kinetic energy is greatly altered by the introduction of the incident shock. The baseline cases show the development of a large region of medium-intensity turbulent kinetic energy that propagates

10
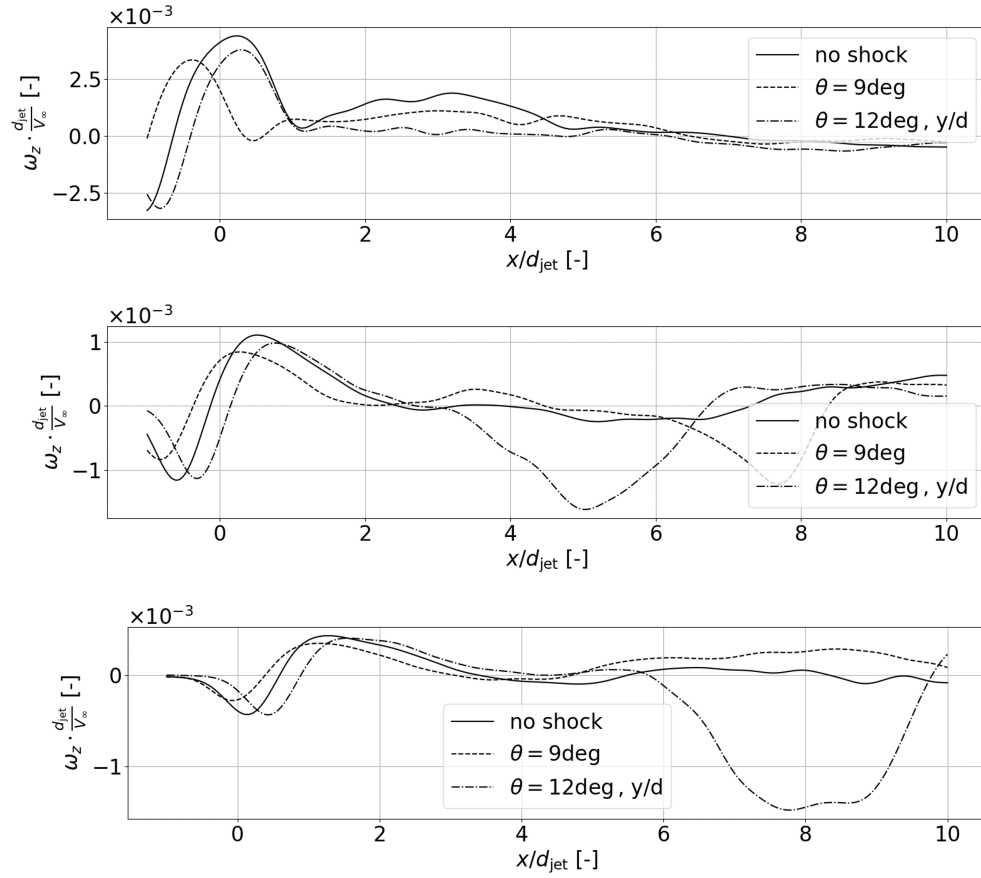
Fig. 13   Vorticity as a function of streamwise distance from injection point at $y/d_{jet} = 1$ **(top),** $y/d_{jet} = 2$ **(middle) and** $y/d_{jet} = 3$ **(bottom). Extracted at** $z = 0$.

upwards and away from the wall. This no longer appears visible when a shock impacts the plume. Instead, a very high-intensity region is seen in the immediate near field of the jet, followed downstream by medium-to-low-intensity flow area, and instantaneous frames still show the abundant presence of shear layer vortices. The injection of transverse momentum into the flow directly upon injection combined with the compression wave generated upstream in the near-to-mid-field of the jet has the effect of bringing injectant high above the wall in the strong shock case. Whereas for the strong shock case this translates into a widespread diffusion of turbulent kinetic energy over a large area, for the 9-degree case the spread is less pronounced. In combination with the fact that a higher shock strength leads to a higher jet penetration in the near field and the increased residence time due to lower velocity through the channel, it can be concluded that the shock wave could potentially have a positive benefit to the mixing performance. However, mixing does not spread much further than the centre-line of the test section. Indeed, as shown in the above, turbulent kinetic energy is mostly concentrated in the developing branches of the CVP, as visualizations in a spanwise offset plane at $z/d_{jet} = \pm 2$ (not shown here) reveal. The bow shock quickly loses its intensity as the plane shifts away from the centre line and, thus, it plays no key role in the off-centre mixing. The only mechanism affecting the evolution of mixing along the spanwise direction is the lateral expansion of the jet plume.

11
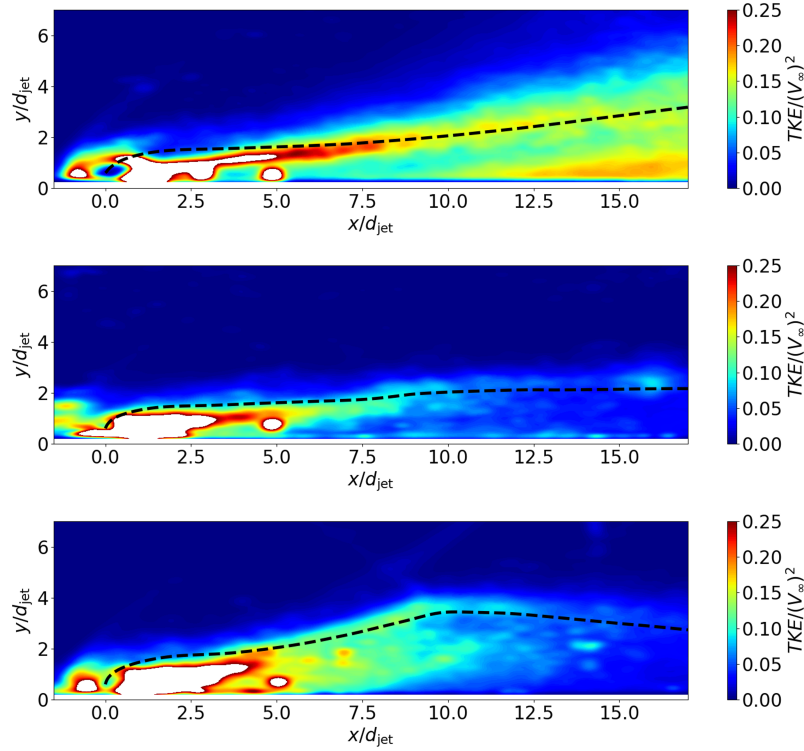
Fig. 14   Turbulent kinetic energy fields for $J = 1$ and no shock impingement (top), $\theta = 9\deg$ (middle) and $\theta = 12\deg$ (bottom). Impingement position $x_{\text{shock}}/d_{\text{jet}} = 13$. Trajectory marked with dashed line.

Another parameter considered in the present investigation is the effect of the impingement location of the oblique shock wave on the plume, characterized by the location where the oblique shock wave would reach the wall in a completely inviscid field. Figure 15 shows the velocity magnitude, vorticity and turbulent kinetic energy fields for the configuration where the shock impinges at the farthest downstream position ($x_{\text{shock}}/d_{\text{jet}} = 16$), whereas all previously shown resuts relate to the more upstream impingement location, corresponding to $x_{\text{shock}}/d_{\text{jet}} = 13$. With the shock impingement location more downstream, a region where the flow appears to accelerate again is visible downstream close to the injector location (between x/d = 2.5 and 7.5), also thanks to the action of the expansion developing over this flow region. The delayed onset of the shock-induced compression wave also causes a weaker shear layer between the jet plume and the surrounding fluid, as evident from the comparison between Figures 12 (bottom) and 15 (middle). A relatively large region of low vorticity is observed between the bow shock wave and the compression wave. This illustrates how the more downstream interaction results in the development of a weaker shear layer along the jet trajectory axis, in comparison to the more upstream interaction (see Figure 12, for instance). Finally, considering the distribution of turbulent kinetic energy, the region of elevated turbulent kinetic energy levels is lower in height and stretches further downstream.
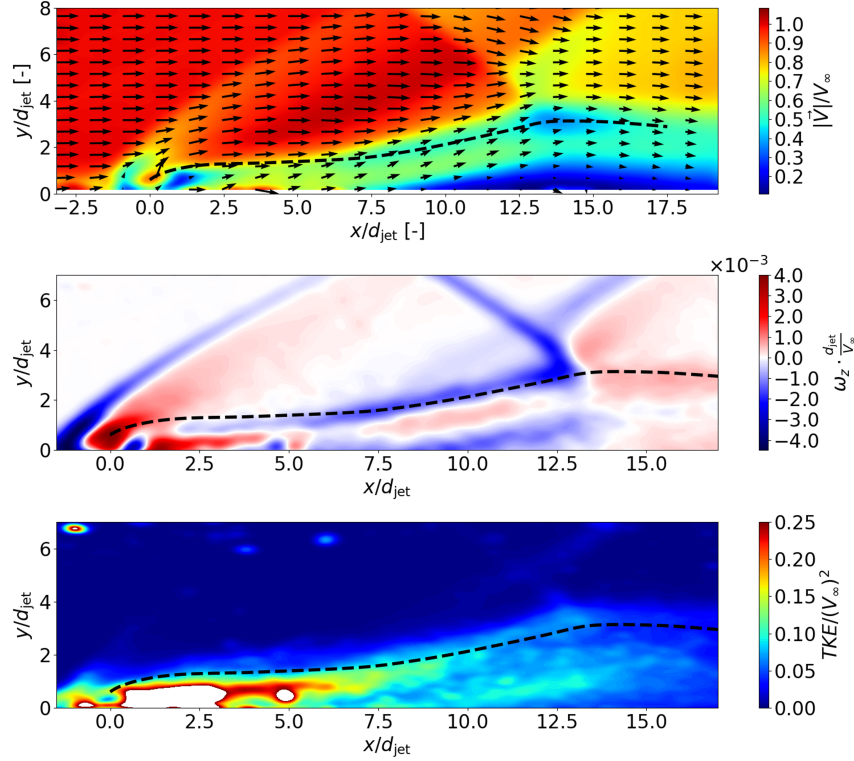
Fig. 15 Velocity magnitude (top), vorticity field (middle) and turbulent kinetic energy (bottom) for $J = 1$, $\theta = 12\,\mathrm{deg}$ and $x_{\mathrm{shock}}/d_{\mathrm{jet}} = 16$.

V. Conclusion

In this study the interaction between an oblique shock and a jet in a Mach 2 cross flow has been investigated experimentally. The influence was investigated of the following three main parameters: the jet's momentum flux ratio (J), the flow deflection angle (θ) and the shock impingement location downstream of the jet injection point ($x_{\mathrm{shock}}/d_{\mathrm{jet}}$). Combined oil flow visualization and schlieren photography have been used in an exploration of the main flow features of the interaction. In addition, stereoscopic particle image velocimetry was carried out for quantitative flow field measurements, in both wall-normal and wall-parallel planes.

From the schlieren visualization a basic characterization of the flow field is obtained, for both the baseline and interaction configurations. Concerning the behaviour of the flow in the near-field of the jet, a barrel shock forms enveloping the exhaust of the nozzle. The position of the Mach disk, of fundamental importance for momentum-driven mixing in the near-field, rises linearly from the wall with increasing J, and simultaneously shifts downstream. According to the literature, a larger distance of the Mach disk from the exit location is beneficial for the mixing performance [20].

The effect of the shock on mixing has a complex nature, with multiple aspects involved. Different flow features can arise, depending on the shock strength and downstream impingement position. The occurrence of a low-speed flow region is beneficial for the entrainment of the two air flows as this generally leads to greater velocity gradients and, thus, vorticity and strain. Two variables were monitored in this study for the quantification of this interaction: the jet trajectory as a measure of the plume's penetration and the turbulent kinetic energy in the flow field.

Jet penetration was shown to increase when a strong oblique shock is introduced. Due to the combined action of the CVP and the upward deflection associated to the compression upstream of the SBLI region, the plume showed an increase in height above the wall, compared to the baseline configuration. In particular, for $J = 1$ and $J = 2$, it showed a 45% and 66% increase in jet height at $x/d_{\mathrm{jet}} = 10$, respectively. This was for the case where $\theta = 12\,\mathrm{deg}$ and $x_{\mathrm{shock}}/d_{\mathrm{jet}} = 13$. Little to no improvement was found for the weaker impinging shock (i.e. $\theta = 9\,\mathrm{deg}$). Moreover, the 12-degree shock case also provides more lateral expansion, as large-scale vortices could be observed both in the $y/d_{\mathrm{jet}} = 1$ and $y/d_{\mathrm{jet}} = 2$ planes, which greatly contribute to entrainment enhancements.

The distribution of turbulent kinetic energy across the flow is greatly affected by the presence of the shock. The area

13

of- high-intensity turbulent kinetic energy is spread over a larger portion of the field compared to the cases with weak shock impingement. Coupled with the observation that the shock wave brings the injectant higher above the wall, it can be concluded that the shock has a net positive benefit on the mixing performance of the jet with the crossflow.

References

[1] Segal, C., *The Scramjet Engine Processes and Characteristics*, Cambridge Aerospace Series, Cambridge University Press, 2009.

[2] Kelso, R. M., Lim, T. T., and Perry, A. E., "An Experimental Study of Round Jets in Cross-flow," *Journal of Fluid Mechanics*, Vol. 306, 1996, pp. 111–144. https://doi.org/10.1017/s0022112096001255.

[3] Morkovin, M., Jr., C. P., and Craven, C., "Interaction of a Side Jet with a Supersonic Main Stream," *Bulletin of Mechanical Engineering of the University of Michigan*, Vol. 35, 1952.

[4] Portz, R., and Segal, C., "Penetration of Gaseous Jets in Supersonic Flows," *AIAA Journal*, Vol. 44, No. 10, 2006, pp. 2426–2429. https://doi.org/10.2514/1.23541.

[5] Zukoski, E. E., and Spaid, F. W., "Secondary Injection of Gases into a Supersonic Flow," *AIAA Journal*, Vol. 2, No. 10, 1964, pp. 1689–1696.

[6] Beresh, S. J., Henfling, J. F., Erven, R. J., and Spillers, R. W., "Penetration of a Transverse Supersonic Jet into a Subsonic Compressible Crossflow," *AIAA Journal*, Vol. 43, No. 2, 2005, pp. 379–389. https://doi.org/10.2514/1.9919.

[7] Beresh, S. J., Henfling, J. F., and Erven, R. J., "Flow Separation Inside a Supersonic Nozzle Exhausting into a Subsonic Compressible Crossflow," *Journal of Propulsion and Power*, Vol. 19, No. 4, 2003, pp. 655–662. https://doi.org/10.2514/2.6154.

[8] Li, L.-q., Huang, W., Yan, L., and Li, S.-b., "Parametric Effect on the Mixing of the Combination of a Hydrogen Porthole with an Air Porthole in Transverse Gaseous Injection Flow Fields," *Acta Astronautica*, Vol. 139, 2017, pp. 435–448. https://doi.org/10.1016/j.actaastro.2017.07.048.

[9] Nakamura, H., Sato, N., Kobayashi, H., and Masuya, G., "Effect of the Location of an Incident Shock Wave on Combustion and Flow Field of Wall Fuel-Injection," *Trans. Japan Soc. Aero. Space Sci*, Vol. 51, 2008, pp. 170–175.

[10] Gerdroodbary, B., Jahanian, O., and Mokhtari, M., "Influence of the angle of incident shock wave on mixing of transverse hydrogen micro-jets in supersonic crossflow," *International Journal of Hydrogen Energy*, Vol. 40, No. 30, 2015, pp. 9590–9601. https://doi.org/10.1016/j.ijhydene.2015.04.107.

[11] Sun, M., Jing, L., Hai-yan, W., Jian-han, L., Wei-dong, L., and Zhen-guo, W., "Flow Patterns and Mixing Characteristics of Gaseous Fuel Multiple Injections in a Non-reacting Supersonic Combustor," *Heat and Mass Transfer*, Vol. 47, No. 11, 2011, pp. 1499–1516. https://doi.org/10.1007/s00231-011-0804-x.

[12] Lee, S.-H., "Characteristics of Dual Transverse Injection in Scramjet Combustor, Part 1: Mixing," *Journal of Propulsion and Power*, Vol. 22, No. 5, 2006, pp. 1012–1019. https://doi.org/10.2514/1.14180.

[13] Babinsky, H., and Harvey, J. K., *Shock Wave-Boundary-Layer Interactions*, Cambridge University Press, 2011.

[14] Humble, R. A., Elsinga, G. E., Scarano, F., and van Oudheusden, B. W., "Three-dimensional instantaneous structure of a shock wave/turbulent boundary layer interaction," *Journal of Fluid Mechanics*, Vol. 622, 2009, pp. 33–62. https://doi.org/10.1017/s0022112008005090.

[15] White, F. M., *Viscous Fluid Flow, Third Edition*, McGraw Hill Series in Mechanical Engineering, McGraw Hill Education, 2011.

[16] Yan, L., Wu, H., Huang, W., Li, S.-b., and Liu, J., "Shock Wave/Turbulence Boundary Layer Interaction Control With The Secondary Recirculation Jet In A Supersonic Flow," *Acta Astronautica*, Vol. 173, 2020, pp. 131–138. https://doi.org/10.1016/j.actaastro.2020.04.003.

[17] Pourhashem, H., Kalkhoran, I. M., and Kumar, S., "Interaction of Vortex with Bow Shock Wave: Computational Model, Experimental Validation, Enhanced Mixing," *AIAA Journal*, Vol. 56, No. 8, 2018, pp. 3071–3085. https://doi.org/10.2514/1.J056789.

[18] Smart, M. K., and Kalkhoran, I. M., "Effect Of Shock Strength On Oblique Shock-Wave/Vortex Interaction," *AIAA Journal*, Vol. 33, No. 11, 1995, pp. 2137–2143. https://doi.org/10.2514/3.12958.

[19] Nakamura, H., Sato, N., Ishida, S., Ogami, Y., and Kobayashi, H., "A Study of Interaction between Shock Wave and Cross-Flow Jet Using Particle Tracking Velocimetry," *Trans. Japan Soc. Aero. Space Sci*, Vol. 52, 2009, pp. 81–88.

[20] Kawai, S., and Lele, S. K., "Dynamics And Mixing Of A Sonic Jet In A Supersonic Turbulent Crossflow," *Annual Research Briefs, Centre for Turbulence Research*, 2009, pp. 285–298.

[21] Yan, L., Huang, W., Li, H., and Zhang, T.-t., "Numerical investigation and optimization on mixing enhancement factors in supersonic jet-to-crossflow flow fields," *Acta Astronautica*, Vol. 127, 2016, pp. 321–325. https://doi.org/10.1016/j.actaastro.2016.06.011.

[22] Chai, X., and Mahesh, K., "Simulations of High Speed Turbulent Jets in Crossflows," 49th AIAA Aerospace Sciences Meeting including the New Horizons Forum and Aerospace Exposition, 2011. https://doi.org/10.2514/6.2011-650.

[23] Dickmann, D. A., and Lu, F. K., "Shock/Boundary-Layer Interaction Effects on Transverse Jets in Crossflow over a Flat Plate," *Journal of Spacecraft and Rockets*, Vol. 46, No. 6, 2009, pp. 1132–1141. https://doi.org/10.2514/1.39297.

[24] Sun, M.-b., and Hu, Z.-w., "Mixing In Nearwall Regions Downstream Of A Sonic Jet In A Supersonic Crossflow At Mach 2.7," *Physics of Fluids*, Vol. 30, No. 10, 2018. https://doi.org/10.1063/1.5045752.

[25] Nedungadi, A., and Lewis, M. J., "Numerical Study of Fuel Mixing Enhancement Using an Oblique Shock/Vortex Interaction," *Journal of Propulsion and Power*, Vol. 16, No. 6, 2000, pp. 946–955. https://doi.org/10.2514/2.5691.